LANGMUIR

pubs.acs.org/Langmuir
Article

High-Performance Roller Tube-Shaped Copper Foam Solar Evaporators with Copper Foil Integration for Enhanced Thermal Control

Husam Eltigani* and Yuttanant Boonyongmaneerat*

Cite This: *Langmuir* 2025, 41, 11794–11805
Read Online

ABSTRACT: The growing global freshwater shortage and climate crisis are increasing the dependence on water desalination technologies. To meet this pressing demand, innovative solutions that utilize renewable energy sources like solar power, with an emphasis on improving evaporation processes, are essential. Although considerable research has been conducted on a variety of materials and structural designs, the development of highly efficient solar steam generators for large-scale use remains a challenge. Here, we introduce a novel design: a two-layer vertical evaporation cylinder in a roll format that integrates a small, inverted cone-shaped pure copper (ICPC) foam and etched copper foil to enhance thermal management. The primary objective is to advance direct solar desalination and interfacial evaporation by effectively capturing both direct and reflected light while preventing salt accumulation through self-cleaning. This design leverages the optical properties of the three materials—absorption, reflection, and transmission—while providing deeper insights into seawater behavior within the foam's interconnected pores. It also addresses common challenges encountered by traditional solar evaporators, such as salt buildup, uncontrolled water flow, and poor thermal management. This cutting-edge solar evaporation system exhibits exceptional performance, remarkable adaptability to diverse configurations, and represents a breakthrough in sustainable chemistry, featuring an advanced engineering design that achieves an outstanding evaporation rate of 17.15 kg·m^{-2}·h^{-1} under 1 sun irradiation.

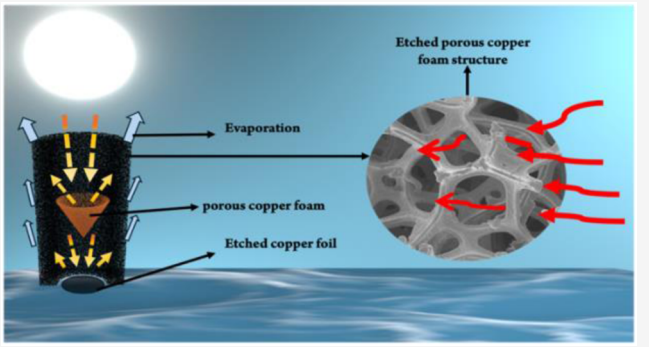

INTRODUCTION

For efficient solar energy harvesting, a proposed system must satisfy the substantial energy requirement for vaporization. The system must efficiently gather and focus this energy to effectively bridge the gap between the high energy demand for processes like vaporization and the solar energy available from the environment. Successful thermal design involves careful materials selection, considering factors such as heat capacity and the physical response of materials, alongside the necessity of being economically feasible and easily fabricated to ensure the effectiveness of the design. For more development, metal foam, endowed with excellent thermal conductivity facilitating efficient heat harnessing control,[1,2] represent a promising avenue for various applications[3] Within this framework, copper foam emerges as a particularly compelling material with excellent corrosion resistance, high thermal conductivity, and mitigation of bacteria[4] which are essential for obtaining efficient water disinfection with high-quality, safe drinking fresh water,[5] and, primarily, for solar-driven evaporation[6] Its ability to rapidly spread heat ensures enhanced performance and durability in evaporation processes, making it an attractive option for harnessing solar energy.

Furthermore, copper foam can serve as a self-supporting framework when combined with CuO nanowires to maximize solar energy absorption.[7,8] Additionally, porous copper foam can be infused with phase change materials (PCMs) and coated with carbon nanoparticles and poly(dimethylsiloxane) (PDMS) to efficiently capture solar energy. The carbon-coated copper foam (CCF) helps prevent PCM leakage while directly absorbing sunlight[9,10] Furthermore, copper foam and functionalized graphene oxide can be used together through a scalable process involving wet oxidation, impregnation, and room-temperature drying. This unique combination provides ample channels for light absorption, improving water movement and vapor diffusion and the development of vaporators with multifunctional capabilities for the cogeneration of freshwater and electricity.[11,12] The pores typically range from 100 to 300 μm in diameter within the approximately 100 μm thick copper

Received: March 17, 2025
Revised: April 22, 2025
Accepted: April 22, 2025
Published: April 30, 2025

https://doi.org/10.1021/acs.langmuir.5c01314
Langmuir 2025, 41, 11794−11805

network[13] Another example involves highly porous reticulated vitreous carbon (RVC) foam combined with copper foam, which offers a high thermal conductivity (34.1 $W{\cdot}m^{-1}{\cdot}K^{-1}$) and micrometer-sized pores that facilitate vapor escape as in a lily inspired hierarchical design.[14,15] The bionic design in this field can be further developed[13,16] with a variety of salts solutions,[17] including those found in industrial high-salinity wastewater.[18,19]

However, in the literature, various three-dimensional (3D) structures have been developed[20] such as 3D aerogel evaporator[21] and Pompon Dahlia-inspired solar evaporators.[22] Several investigations have also focused on vertical cylindrical shapes—for example, a 10 cm cotton core wrapped in plant cellulose and dip-coated with carbon black nanoparticles (20 g/L in ethyl alcohol) on both the top and side surfaces, as demonstrated by Li and his team[23] to reach an evaporation rate of 1.47 $kg{\cdot}m^{-2}{\cdot}h^{-1}$ under 100 $mW{\cdot}cm^{-2}$. Another example Wang et al. produced vertically ordered channels in biomimetic aerogels consisting of ultralong hydroxyapatite nanowires as heat-insulating skeletons and polydopamine-modified MXene as a photothermal material yielded an evaporation rate of 2.62 $kg{\cdot}m^{-2}{\cdot}h^{-1}$ with 93.6% energy efficiency.[24,25] In similar case, fabricated vertically aligned *Juncus effusus* on fibril skeleton by Zhang et al.[26−28] as a solar evaporator to achieve an evaporation rate of 2.23 $kg{\cdot}m^{-2}{\cdot}h^{-1}$ under 1 sun illumination. In case of polymer materials, Li et al.[29] introduced a vertically π-extended acceptor unit, polymers achieved absorption peaks over 1000 nm. This polymer E-DTP had covering 300−1700 nm, was dip-coated on a melamine sponge, forming a Janus evaporator with an evaporation rate of 2.10 $kg{\cdot}m^{-2}{\cdot}h^{-1}$ and 86.9% solar-to-vapor efficiency under 1 sun. Other approaches include using a double layer of the polymer polypyrrole (PPy) due to its excellent light-absorbing ability, along with PVA species that correspond to different degrees of polymerization[30] or employing a dual-network hydrogel (DNH) with a hierarchical structure featuring alternating pore sizes. By fine-tuning the amide groups within the hydrogel network, the DNH—rich in hydrophilic functional groups (−OH and $-CONH_2$)—promotes ionic diffusion equilibrium, achieving an evaporation rate of 4.0 $kg{\cdot}m^{-2}{\cdot}h^{-1}$ under 1 sun.[31]

Moreover, more economically with the inspired from nature such as the use of the corncob structure by Sun et al.[32] This 3D carbonized corcob (C-corncob) with vertical cylindrical shape was harmoniously coordinates light absorption achieved a water evaporation rate of 4.16 ($kg{\cdot}m^{-2}{\cdot}h^{-1}$) under 1 sun. Similar by using natural resource material, Wani el al.[33] produced carbonized coconut husk evaporators in a vertical shape, with fibers bonded by spongy coconut pith, maintained their structure after carbonization, resulting in a solar evaporator achieving evaporation rate of 3.6 $kg{\cdot}m^{-2}{\cdot}h^{-1}$ with 90.2% efficiency. In another example, Dang et al.[34] soaked rattan wood in a mixed solution of 2.5 M NaOH and 0.4 M Na_2SO_3 at 95 °C for 8 h to obtain a vertical shape with multichannel and antigravity water transportation, achieved an average high evaporation rate of 30.24 $kg{\cdot}m^{-2}{\cdot}h^{-1}$. In addition, rattan wood has been advanced as a salt-resistant 3D solar evaporator with elevated structure and well-aligned fluid channels across multiple scales. This design enables faster water replenishment at the evaporation surface and streamlines salt backflow pathways, effectively enhancing salt circulation and addressing the persistent issue of salt buildup.[35] Further developments include the use of a 3D vertical graphene oxide stalk, with the main structure originating from a cotton rod[36] such as the one fabricated by Finnerty et al.[37] This structure was processed through a sequence of dip-coating, flash freezing, and freeze-drying, then cross-linked and assembled in a vertical configuration, achieving an evaporation rate of 34.7 $kg{\cdot}m^{-2}{\cdot}h^{-1}$ under 1 sun (1 kW/m^2). However, despite these advances, challenges remain in creating easily fabricated solar evaporators[38] with assembled and repairable components and rigid structures suitable for more real applications such as wastewater treatment. In addition, there is a need for further improvement in managing heat distribution within the internal structure, rather than focusing solely on the external surfaces, to ensure more effective thermal management and greater operational versatility.

In this study, we developed a novel double-layer tubular roller copper foam design that can be optimized and reproduced for enhanced thermal management. The design not only addresses key challenges in heat distribution but also provides deeper insights into the role of interconnected pores in facilitating efficient heat penetration—an aspect rarely explored in the existing literature. This innovative 3D vertical architecture strategically integrates three materials in an economical manner to minimize energy loss. To the best of our knowledge, this is the first study to systematically investigate the tuned, distinct light interaction properties of copper foam, etched copper foam, and etched copper foil within a single structure. By examining their effects on solar absorption, emittance, and reflection, we also evaluate their influence on evaporation rates, water transport dynamics, and salt accumulation—critical factors in sustainable desalination technologies. This approach enhances light trapping and internal heat distribution rather than concentrating heat solely on external surfaces.

EXPERIMENTAL WORKS

Material Selection and Design. Aiming to develop evaporator structures for long-term use with scalability and practical applicability, we selected copper foam as the primary material for several reasons. Copper is unique as the only known catalyst capable of directly converting CO_2,[39] copper foam can be combined with other materials to enhance thermal control hardware of various sizes,[40] easily manufactured and serving as a framework to prevent the separation of metal particles[41] Compared to other materials, copper foam also ensures greater rigidity and longevity, addressing fabrication challenges when scaling up.[42,43] More importantly, in seawater applications and long-term realistic scenarios where seawater is contaminated with oil—an issue frequently occurring in various regions—copper foam is a preferred choice for efficient oil−water separation. It achieves up to 98% separation efficiency after 40 cycles, in contrast to other materials that may struggle to handle contaminated seawater environments effectively.[44,45]

Moreover, to ensure efficient seawater transport to the evaporation area, the wettability of copper foam surfaces must be adjusted.[46,47] This can be achieved using techniques such as hot alkaline treatments or femtosecond laser processing, as demonstrated by Yin et al., who achieved a water evaporation rate of approximately 7.6 $kg{\cdot}m^{-2}{\cdot}h^{-1}$ under one-sun irradiation.[48] Copper foam can also be methodically coated with a hydrophilic poly(vinyl alcohol) (PVA) aerogel (ACPA) mixture by saturating the foam with a PVA/chitosan solution, followed by freeze-drying and subsequent acetylation in acetic anhydride[49] Additionally, the copper foam surface can be oxidized to form black CuO, followed by dip-coating with a blend of CuS nanoparticles (CuSNPs) and agarose gel (AG) to enhance near-infrared (NIR) absorption and water transport.[50] However, in this work, we used chemical etching to modify the surface to be superhydrophilic for enhanced water transport while simultaneously achieving a blackened surface to maximize solar energy absorption. We also chemically etched copper foil to serve as a heat storage layer, adding heat retention properties to the bottom of the proposed evaporators. Furthermore,

https://doi.org/10.1021/acs.langmuir.5c01314
Langmuir 2025, 41, 11794−11805

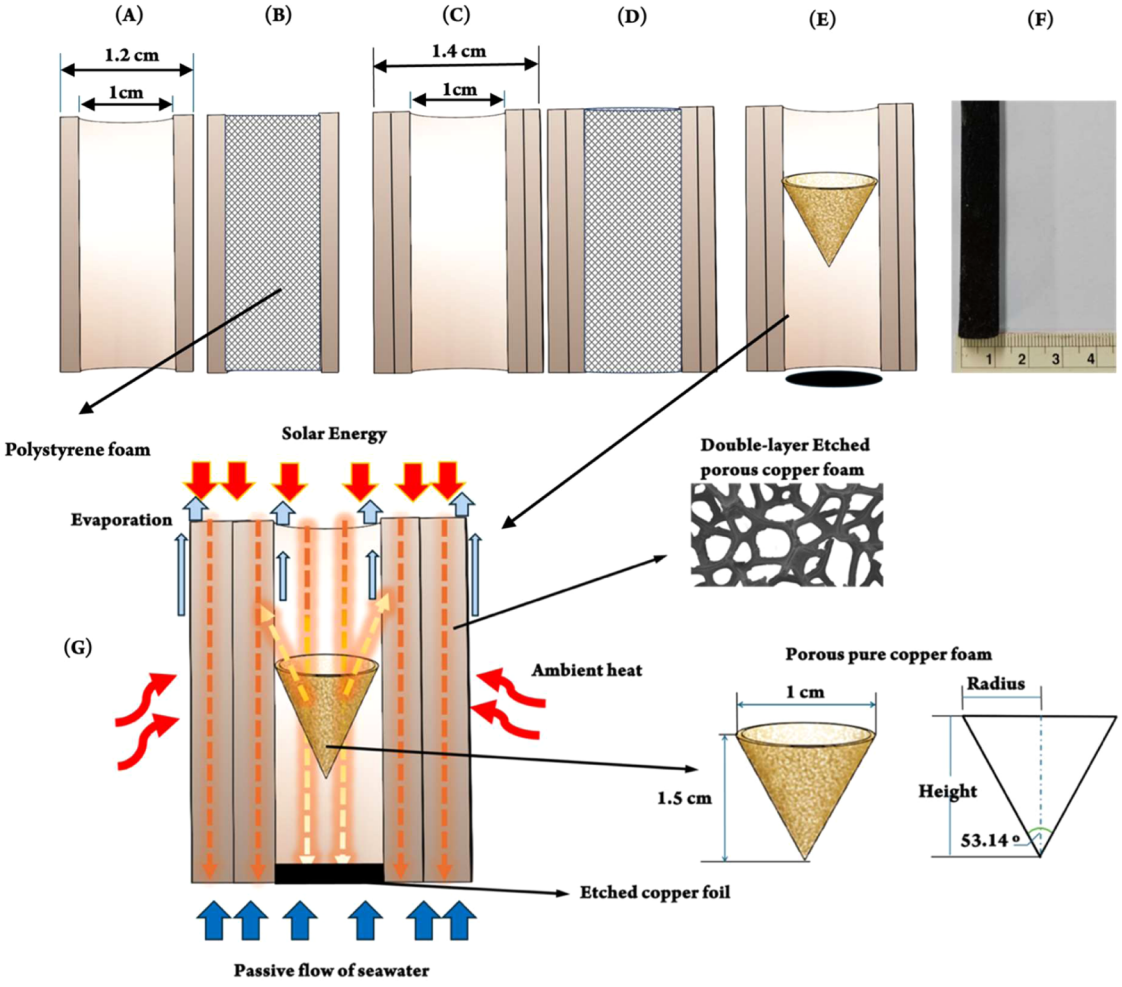

Figure 1. (A–D) Cross-sectional schematics of single- and double-layer evaporators with and without polystyrene foam filling. (E) Optimized evaporator structure integrating ICPC foam and etched copper foil for improved efficiency. (F) Real photograph measuring the single-layer evaporator's diameter. (G) Overview of optimized structure and ICPC foam geometrical dimensions.

artificial seawater (3.5% NaCl) was introduced at one end of a porous medium (etched copper foam), while vapor escapes from the top area on the opposite side and near the wall. This process is known as Phase -Change Transpiration cooling.[51,52]

Most importantly, the limit of water lifting is associated with the properties of porosity and the height of the cylinder. In all the samples, the height is limited to around 5 cm for a pore density of 100 PPI, which can be increased by using a higher PPI. There is also the possibility of using other copper foam densities in this field, such as copper foam with 110 PPI[42] or 130 PPI.[13] However, in terms of structural design, various designs reported in the literature—such as cones,[53] inverted cones as a whole structure,[54] pyramid shape,[55] and two-dimensional (2D) flat surfaces[56]—have been explored. While each of these designs offers unique advantages, they may also encounter challenges related to salt accumulation and suboptimal heat distribution throughout the structure.

A vertical cylindrical design with double rollers and a 3D shape offers greater scalability. More importantly, for practical use in large-scale constructions, it conserves land space compared to 2D flat surfaces, which require a larger footprint when scaled up. Additionally, out design effectively addresses common challenges such as continuous seawater transport and the unobstructed movement of water vapor away from the evaporator. For comparison, polystyrene foam was used in both single-layer and double-layer configurations to fill the empty spaces. In certain setups, the presence of a central polystyrene foam component within the evaporator resulted in a structure resembling a solid cylinder, enabling an assessment of the effect of a roller-like evaporator design versus an unfilled structure in single-layer and double-layer evaporators, as shown in Figure 1(A–D).

Moreover, a small, inverted cone-shaped piece of pure copper foam ICPC with a hydrophobic surface was integrated into the main structure, as shown in Figure 1E with geometrical dimension of ICPC. The total fabrication cost, including materials and chemicals, was approximately ($3.78) with more details of cost analysis in Table S5. This cost-effective addition enhances heat penetration by reflecting light into the interior, while the etched copper foil helps retain heat at the bottom of the structure. Compared to previous studies in the literature that employed solid metal cylinders—where heat primarily benefits only the outer interfacial layer near the top and side surfaces exposed to the environment—this approach ensures better heat distribution throughout the entire structure, preventing untreated interior regions. To minimize heat loss into the bulk water, low thermal conductivity polystyrene foam was used to cover the beaker, ensuring that water transport occurred exclusively through the evaporator.

Samples Preparation. The copper foams were commercially purchased and are easily foldable, with a pore density of 100 PPI and a mechanical strength around 2.5 MPa. The wall thickness of the fabricated cylindrical shape is 1.0 mm, with an outer diameter of 12 mm and an inner diameter of 10 mm. The skeleton of the copper foam samples was modified using a chemical oxidation process in an alkaline solution, creating a uniform copper hydroxide layer to enhance wettability and ensure continuous water transport to the evaporation area by immersing the samples in a solution containing sodium hydroxide and ammonium persulfate. We modified the procedures reported in the literature[57−59] by adjusting the etching temperature to

https://doi.org/10.1021/acs.langmuir.5c01314
Langmuir 2025, 41, 11794−11805

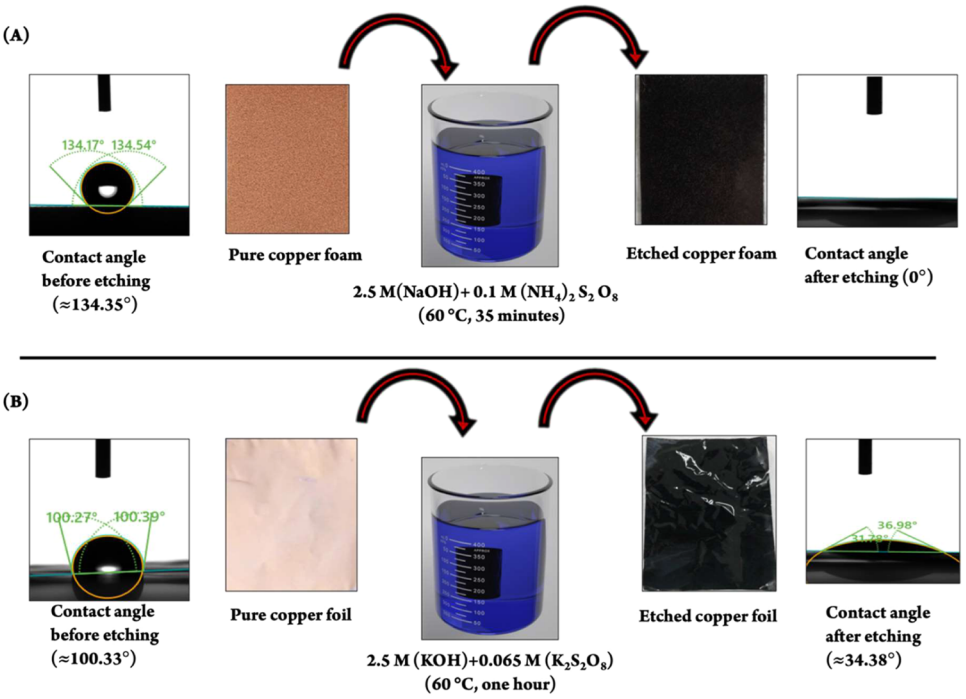

Figure 2. Surface wettability modification by chemical etching: (A) Copper foam before and after etching, showing changes in artificial seawater contact angle. (B) Copper foil contact angle before and after etching.

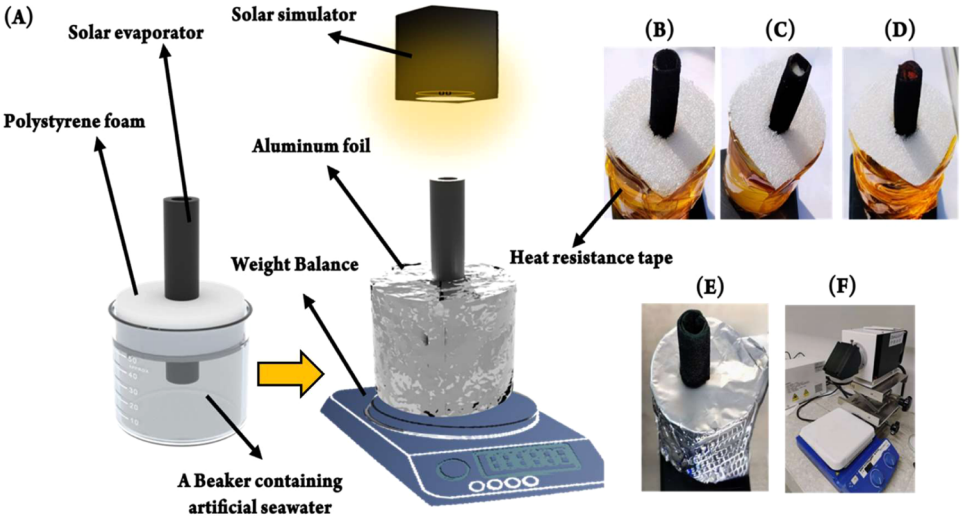

Figure 3. Experimental setup and solar evaporator configurations: (A) Schematic of the testing setup. (B–D) Real solar evaporators before aluminum foil covering: (B) single-layer, (C) filled with polystyrene foam, and (D) optimized structure with ICPC inserted in the empty space. (E) Fully covered evaporator with aluminum foil after applying heat-resistant material. (F) Solar simulator used for evaporation rate testing.

60 °C and the duration to 35 min. The preparation process of copper foam samples started with cleaning process using a 5% hydrochloric acid (HCl) solution mixed with DI water to remove any oxide layers on the copper foam, followed by rinsing with DI water. The cleaned cylindrical copper foams are then immersed in a solution of 2.5 M sodium hydroxide (NaOH) and 0.1 M ammonium persulfate ($(NH_4)_2S_2O_8$), as shown in Figures 2A and S1 in Supporting Information file. After treatment, the samples were air-dried at room temperature for 24 h. This chemical reaction forms copper hydroxide, which exhibits superhydrophilic properties due to the presence of hydroxide groups (OH−).

The reaction equation is as follows

$$Cu + 4NaOH + (NH_4)_2S_2O_8 \rightarrow Cu(OH)_2 + 2Na_2SO_4 + 2NH_3 + 2H_2O \quad (1)$$

For copper foil, we found that the KOH and $K_2S_2O_8$ solution was more suitable for obtaining hydrophilic etched copper foil as shown in Figure 2B, following procedures reported in various references.[35,36] Scanning electron microscopy was used to compare the structures obtained with both solutions, starting with the characterization of pure copper foam (Figure 3A). Furthermore, it is important to highlight that when using KOH and $K_2S_2O_8$ with copper foam noticeable residues were observed during etching, along with a clear indication of reduced skeleton thickness (Figure 4B) compared to pure copper foam (Figure 4A). However, when using an alternative solution (NaOH and $(NH_4)_2S_2O_8$), higher concentrations of oxygen and carbon were

https://doi.org/10.1021/acs.langmuir.5c01314
Langmuir 2025, 41, 11794−11805

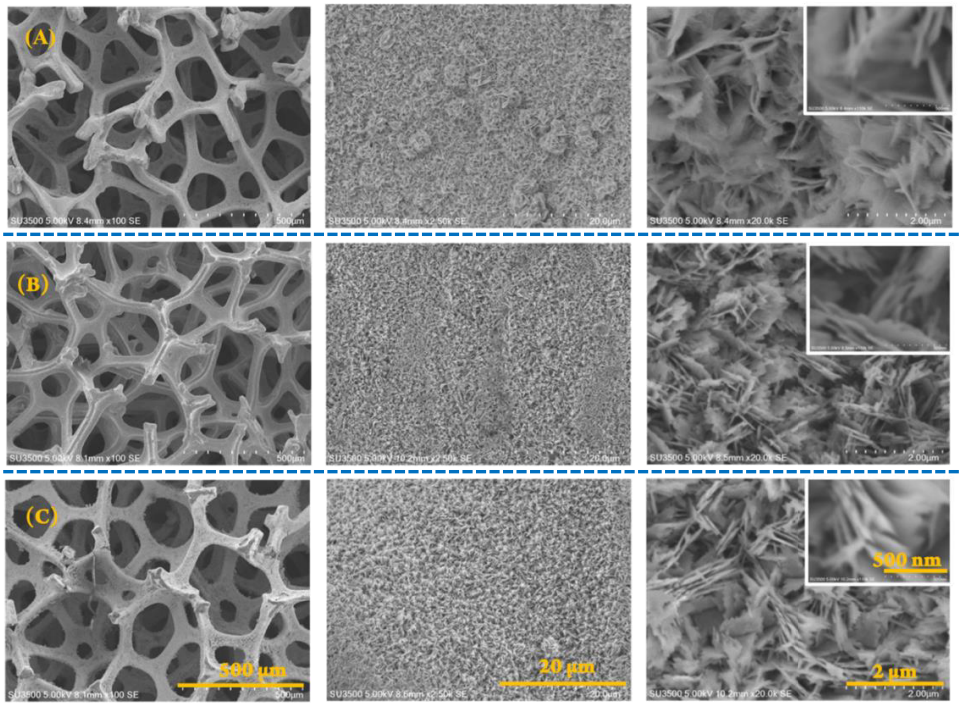

Element	Weight %	Atomic %
C	6.26	25.75
O	0.59	1.83
Cu	93.15	72.42

Element	Weight %	Atomic %
C	4.14	17.67
O	2.09	6.69
Cu	93.77	75.65

Element	Weight %	Atomic %
C	8.17	19.76
O	28.21	51.18
Cu	63.61	29.06

Figure 4. SEM images and EDX elemental contents for (A) pure copper foams, (B) etched copper foams using (KOH and $K_2S_2O_8$), (C) etched copper foams using (NaOH) and ($(NH_4)_2S_2O_8$).

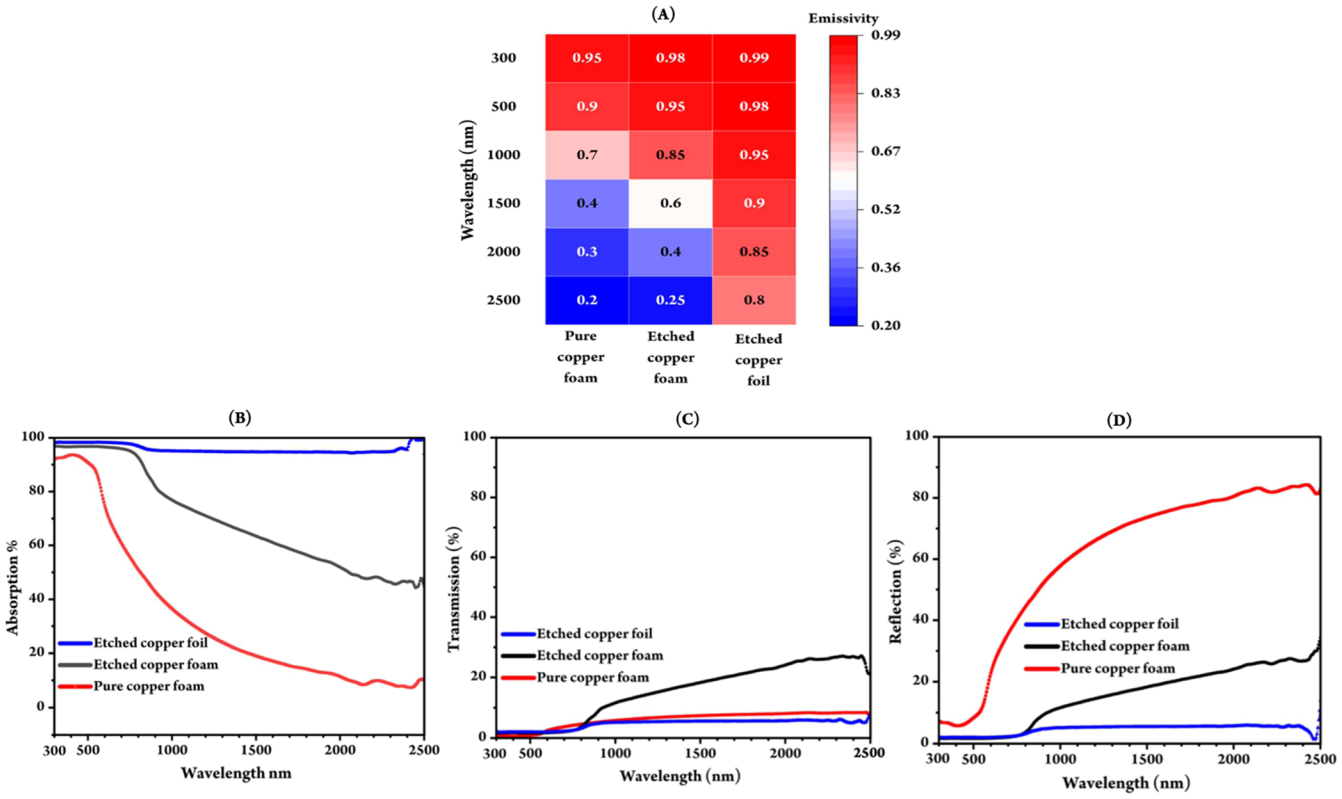

Figure 5. (A) Heatmap of the emissivity of pure copper foam, etched copper foam and etched copper foil, and (B–D) absorption, transmission,and reflection properties in the wavelength range of 300–2500 nm for the three samples, respectively.

observed, forming an added layer of copper hydroxide. This was confirmed by EDX weight ratios of 63.61% copper, 28.21% carbon, and 8.17% oxygen, as shown in the table next to Figure 3C.

Materials Characterization and Testing Setup. The scanning electron microscopy SEM and EDX (Hitachi SU3500) were utilized to examine the surface structure of pure copper foam and etched copper foam. Moreover, the thermal diffusivity and conductivity were determined using the NETSCH Laser Flash Analyzer (LFA 447).[60] The water contact angle (WCA) and ultrafast behavior of a water droplet on the foam surface were measured using a contact angle

https://doi.org/10.1021/acs.langmuir.5c01314
Langmuir 2025, 41, 11794–11805

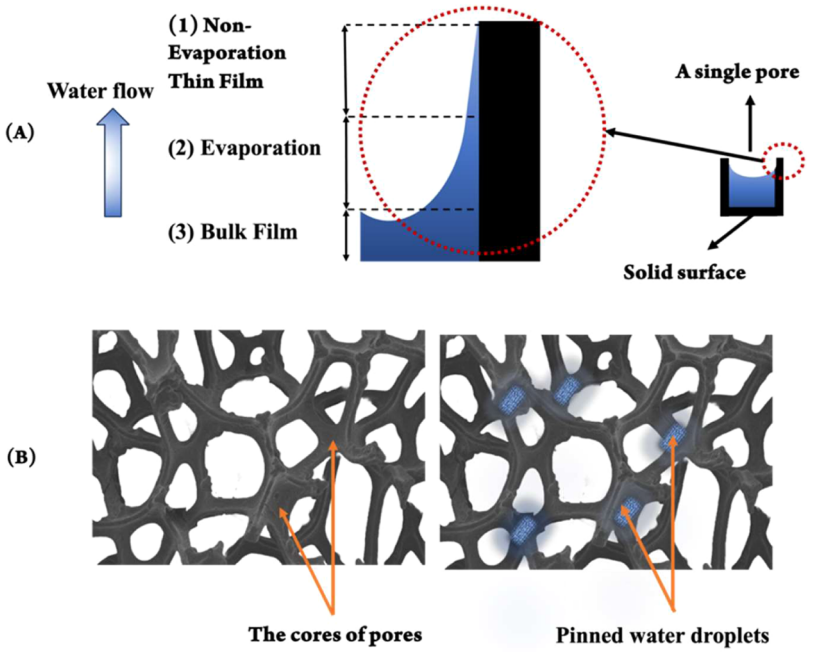

Figure 6. Schematic of water droplet behavior in metal foam pores: (A) Three distinct regions of water droplet interaction with the solid area of a pore. (B) Possible pinning of water droplets within the core of metal foam pores.

goniometer (DataPhysic). Furthermore, the UV−vis spectrophotometer (ERKIN ELMER LAMBDA 950) was used to characterize the absorption, reflection and transmission spectra of the three materials: copper foam, etched copper foam and etched copper foil in the wavelength range of 300 to 2500 nm. Furthermore, infrared photographs and temperature distributions were recorded using an IR camera to capture the temperature of different areas during the evaporation process. A uniform solar flux (1000 $W{\cdot}m^{-2}$) was provided by a solar simulator and a pyranometer was used to measure the light intensity.

The general setup mainly consisted of a vertical etched copper foam roller, a beaker, polystyrene foam, heat resistance tape, and aluminum layer covering all parts except for the exposure area of each evaporator as shown in Figure 3A. Moreover, low thermal conductivity polystyrene foam was used to reduce heat loss into the bulk water. For each experiment, each evaporator was floated in a 60 mL beaker containing 50 mL of artificial seawater (3.5% NaCl). The bottom of each evaporator was immersed in bulk seawater inside the beaker to a depth of 2 cm to ensure a consistent water supply to the evaporating surface via capillary action. Therefore, the height was determined based on the maximum lifting of seawater, set at 5 cm, and remained constant for all samples. Realistic photographs of the single layer, the single layer filled with polystyrene, and the one with ICPC inserted before covering with aluminum foil are shown in Figure 3B−D, respectively. Figure 3E shows the double layer with the final covering of aluminum foil, while Figure 3F displays the solar simulator used for testing the evaporation process of each sample. The weight balance was used to measure the mass change due to evaporation before and after exposing to a solar simulator for 1 h. The change in mass due to evaporation for each sample was measured 3 times, and the average value was taken to minimize experimental errors. For comparison, testing started with a single etched copper foam (SCF), followed by a double-layer (DLC) foam, and continued until reaching an optimized structure with of the small piece of ICPC foam and etched copper foil.

Optical Properties of the Tested Samples. We carried out optical properties, in the wavelength range of 300 to 2500 nm spectra of the three materials using UV−vis spectrophotometer (ERKIN ELMER LAMBDA 950): copper foam, etched copper foam and etched copper foil. Figure 5A−D show heatmaps of the emissivity for all samples, highlighting the differences in optical properties—absorption, transmission, and reflection—between the three materials used to optimize the structure, respectively. The optical characterization of the three samples—pure copper foam, etched copper foam, and copper foil—revealed that copper foil has the best solar absorption capability but low emittance and reflection. In contrast, pure copper foam exhibited a high reflection property, while etched copper foam demonstrated strong absorption and relatively optimal transmission properties, making it ideal for the main structure of the evaporator. From these properties we used the cone-shaped copper foam not only to reflect light to different areas within the foam tube, but also downward trapped heat absorbed by the bottom etched copper foil layer, creating a heat storage effect between the two components. More details in Figure S3 in the Supporting Information. To ensure that the light does not reflect directly upward but instead spreads out across the etched copper foam cylinder, we have carefully obtained the optimal angle for reflection by selecting the slope and geometry of the cone, the height H and the diameter of cone which must be proportional to the inner diameter of the main structure cylindrical shape of the etched copper foam with more details in Supporting Information file (Supporting Note). Additionally, an etched copper foil with broad light spectrum properties (300−2500 nm) as shown from Figure 5A was embedded at the bottom, serving as an efficient heat storage layer.

RESULTS AND DISCUSSION

Water Molecules Behavior within the Foam. The stronger the adhesion of water to the foam skeleton, the lower the evaporative heat transfer flux due to the strong interaction between seawater molecules and the copper foam surface.[61−63] However, utilizing heat flux from sunlight and the surrounding environment with good thermal management, the passage of heat through the network of pores can expand the evaporating thin-film region, as conductive heat reduces adhesion in the nonevaporative areas as shown in Figure 6A. Additionally, within the foam structure, seawater droplets exhibit unstable directional spreading within the pores (slip effect),[64] preventing adhesion to specific areas and allowing for more effective heat absorption.[65] This result ultimately improves thermal management between the structure and the surrounding medium, promoting efficient vapor bubble formation.[66,67] It should be mentioned that a longer conduction path increases thermal

https://doi.org/10.1021/acs.langmuir.5c01314
Langmuir 2025, 41, 11794−11805

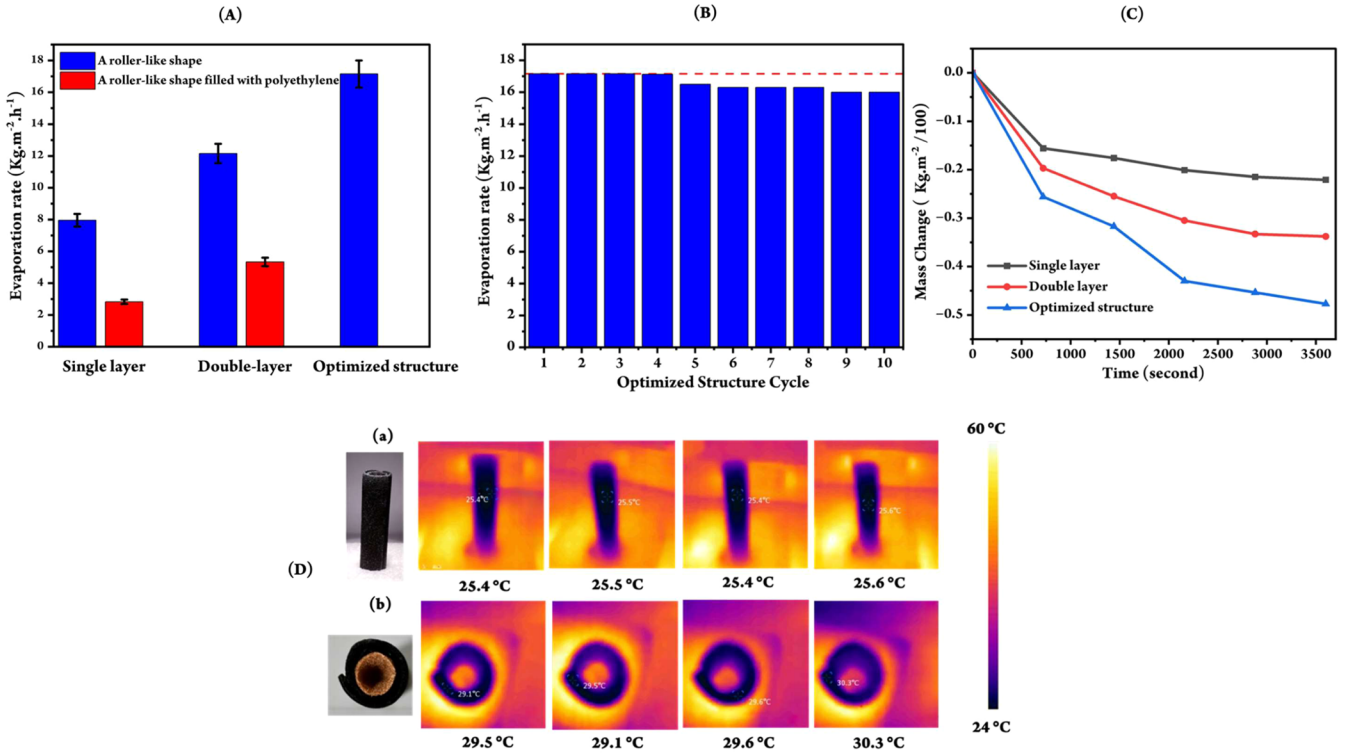

Figure 7. (A) Evaporation rate for a single layer, double layer with and without polystyrene foam filling, and the optimized structure. (B) Optimized structure cycle. (C) Mass change of three samples—single layer, double layer without polystyrene filling, and optimized structure—over 3600 s. (D) Relative temperature stability of the side (a) and top area (b) of the optimized structure throughout the evaporation process.

resistance,[68] lowering the evaporation rate. This is one of the reasons we introduced a design with a double layer and a small piece of ICPC foam capable of converting incident solar radiation along the interior structure. Additionally, the water pathways, porosity, and superhydrophilicity enable better distribution of seawater within the pores, allowing for efficient heat transfer even at the nanoscale voids of the copper foam skeleton, rather than just at the surface edges.

Another remained challenge has not being noted in the literature in the developing in solar desalination system is the tendency of water molecules tending to be pinned in the core of pores as shown in (Figure 5B), a phenomenon called the "pinned effect".[69,70] It is essential to increase the awareness about it especially for system with flat horizontal structure as this phenomena can lead to no empty space for subsequent water molecules lifted during water transport as it may push the upcoming water molecules to the outermost exposure area at the border of the foam, potentially resulting in bulky layers of seawater with the interconnected pores[71] that add more thermal resistance. This hindrance can impede the enthalpy required for evaporation under low sunlight conditions,[72] as increased heat loss occurs due to bulky layers formed at the wall, which resist evaporation. This effect is particularly pronounced when the energy input is insufficient (approximately 1 $kW{\cdot}m^{-2}$), potentially making it inadequate for the phase transition to vapor.[73] However, in our design with a roller shape like evaporator make pinned seawater droplets on the inner surface of the etched copper foam tube have more opportunities for evaporation, as thermal diffusion through the foam ensures sufficient heat transfer and rapid mass change. Moreover, the hierarchical vertical structure, which is consistent in our samples with an open area, reduces interfacial thermal resistance[74] along the radial direction. This lowers the likelihood of pinned molecules due to gravity, decreases the formation of a vapor blanket between the heated surface and the pumped seawater, and triggers the detachment and movement of a drop on a solid surface. Finally, the arrangement of micro/nanostructures effectively regulates heat flow at the interface while enhancing anticlogging properties through precisely tailored pore sizes at the nano/micro scale, as demonstrated in the SEM images shown in Figure 4. Furthermore, surface textures, including micro- or nanoscale features, can also induce pinning effects.[75] If the core surface (the inner wall of the pore) is hydrophilic, it can enhance pinning,[76] as water tends to cling to these surfaces. The roughness inside the pore—including micro/nanostructures—can create contact line hysteresis, which is the essence of pinning. As water is pulled tightly into smaller pores, the contact line (where solid, liquid, and vapor meet) becomes more anchored. This leads to stronger contact line hysteresis, meaning more force or heat is needed to move the droplet. However, when comparing a flat design to a vertical one, the vertical configuration in comparing with horizontal benefits from gravity, which assists in overcoming the pinning effect by facilitating water movement. In the vertical setup, gravity assists in pulling water downward, promoting continuous flow through the pores and reducing the likelihood of droplets becoming pinned within the pore core.[77,78] On horizontal surfaces, small droplets are more likely to be trapped by capillary forces[79] as surface tension dominates over gravity at small scales. Due to their higher surface-to-volume ratio, smaller droplets are more strongly influenced by surface interactions.[80,81] Moreover, it is worth mentioning that intermittent drying of the porous layer decreases as the thickness of the porous layer increases,[82−84] which provides an additional reason for using a double layer of etched copper. However, further increasing the thickness leads to vapor bubbles becoming trapped within the foam cells.[85−87]

https://doi.org/10.1021/acs.langmuir.5c01314
Langmuir 2025, 41, 11794−11805

Salt Accumulation and Self-Cleaning Mechanism. Salt accumulation is significantly minimized during the evaporation process due to the vertical design of our samples, which utilizes gravity to facilitate the removal of salt from the evaporator. This vertical orientation allows the salt to naturally drop outside the evaporator, thereby reducing the risk of accumulation. This design optimizes the balance between water transportation and evaporation rates, leading to a more efficient process overall. Unlike flat-surface evaporators, where salt deposits can easily return to the bulk artificial seawater in the beaker, the unique roller-shaped structure of our design actively prevents this issue by directing the salt away from the evaporator's critical surfaces. Additionally, the tubular design plays a crucial role by promoting continuous water replenishment, which further reduces the likelihood of excessive salt buildup. This dynamic replenishment minimizes stagnant regions that could lead to salt accumulation, a problem often observed in traditional evaporator configurations.

Furthermore, the controlled evaporation rate in our system ensures sustained efficiency over an extended period. While the design significantly reduces salt accumulation, a minimal amount is observed after prolonged operation. Notably, this accumulation is primarily confined to the top surface, where evaporation rates are highest, while the rest of the structure remains largely unaffected. However, after 10 evaporation cycles, a small amount of salt was detected on the sidewall of the etched copper foam This minor accumulation does not significantly impact overall system performance, indicating that the design remains highly efficient even after repeated cycles as shown in Figure 8B. The ability to sustain consistent operation across multiple cycles is critical for practical applications, particularly in regions that require continuous saltwater desalination over extended periods. These findings, along with the self-cleaning capability of our design, highlight the advantages of the roller-shaped evaporator in minimizing salt buildup and ensuring long-term operational efficiency (see Supporting Information, Figure S5). Unlike traditional foam solid cylinders, which are more susceptible to internal salt accumulation, our design prevents the obstruction of seawater transport and maintains consistent light penetration. Over time, trapped salt within foam solid cylinders can clog water pathways, reducing the evaporation rate and limiting heat absorption. In contrast, the roller-shaped evaporator promotes efficient salt removal, preventing deposits from interfering with the desalination process. This comparison emphasizes the superior effectiveness of our roller-shaped evaporator in addressing common challenges related to salt accumulation in solar-driven desalination systems. By maintaining consistent evaporation rates and minimizing performance degradation, this design offers a highly efficient, reliable, and long-lasting solution for practical desalination applications.

It is worth mentioning that even a small amount of salt buildup can reflect sunlight, block vapor escape, and reduce the evaporation rate to around 16 kg/m^2·h, as shown in Figure 7B, starting from cycle 4 and continuing with relatively stable performance up to 10 cycles. Salt accumulation on the evaporator surface significantly affects performance by scattering and reflecting incoming sunlight, thereby reducing light absorption and heat generation. Additionally, salt crystals can obstruct vapor escape pathways, hindering the transport of water vapor from the heated interface to the surrounding air. However, building on the current design, further development of the self-cleaning mechanism can effectively prevent salt accumulation and enable long-term stability. A well-designed network of interconnected pathways enhances ion mobility, helping to maintain a clean and efficient evaporation surface.

The Impact of Interfacial Evaporation. Vapor diffusion into the ambient air is significantly influenced by the expansion of the vapor−liquid interface, which occurs both around the evaporator and within its stagnant inner region of our optimized structure. Since both the outer and inner surfaces of each evaporator are in direct contact with air, the most exposed boundaries of the foam's skeleton provide an extended liquid−vapor interface. This enhanced interface promotes greater vapor diffusion, as a larger surface area allows more seawater vapor to escape. To investigate the impact of interfacial evaporation in the optimized structure, we filled the inner space with polystyrene foam as shown before in Figure 1. This presence of polystyrene foam resulted in a notable 63% decrease in the evaporation rate, primarily due to the restricted entry of ambient air and the reduced permeability of heat through the structure. Furthermore, the polystyrene foam prevented light reflection from penetrating the inner structure, which in turn led to inadequate heat penetration and an imbalance in the water transport rate. As a result, a thicker unevaporated moisture layer accumulated, forming a moisture blanket that obstructed solar irradiation. Under these conditions, even sunlight at 1 kW/m^2 was insufficient to sustain evaporation. Conversely, when the inner space was left empty, warm air in the stagnant region and near the side circumference of the roller structure played a crucial role in the evaporation process. The presence of an empty space facilitated natural convection, allowing less dense, warm air to rise and be replaced by cooler, denser ambient air, thereby maintaining continuous heat transfer. This density gradient induced buoyant forces, further enhancing the evaporation process. Additionally, the notable temperature contrast drove evaporation by drawing heat from the surroundings into the evaporator, involving multiple mechanisms such as heat transfer, surface area interactions, and water vapor diffusion. This temperature differential could also induce the Marangoni effect.[31,88,89]

Moreover, local convective heat transfer occurred on both the interior and exterior walls of the etched copper foam, where a greater temperature contrast enhanced the efficiency of the evaporation process. The heat radiated from the structure warmed the surrounding air, reducing its density compared to ambient air. This density difference drove natural convection, where the warmer air in the empty space created a buoyancy effect, promoting continuous heat transfer to the seawater molecules. This process was hindered when the space was filled with polystyrene foam, as it disrupted natural convection and heat exchange. Therefore, the replenishment of water molecules within the core pores was further enhanced by reflected sunlight from the ICPC foam, which continued to pass through the double layer. The etched copper foam, with its favorable light transmission properties (Figure 5C), enabled more efficient energy absorption and transfer, supporting sustained evaporation performance.

Ultimately, the larger surface area facilitated greater vapor escape, preventing vapor accumulation and enhancing diffusion.[90,91] As a result, the optimized roller structure achieved a significantly higher evaporation rate (17.15 kg·m^{-2}·h^{-1}) compared to the single-layer evaporator (7.96 kg·m^{-2}·h^{-1}) and the double-layer evaporator (12.16 kg·m^{-2}·h^{-1}), as seen in Figure 7A,C. For further insights, readers are encouraged to refer to studies on cylindrical-shaped solid evaporators in the

https://doi.org/10.1021/acs.langmuir.5c01314
Langmuir 2025, 41, 11794−11805

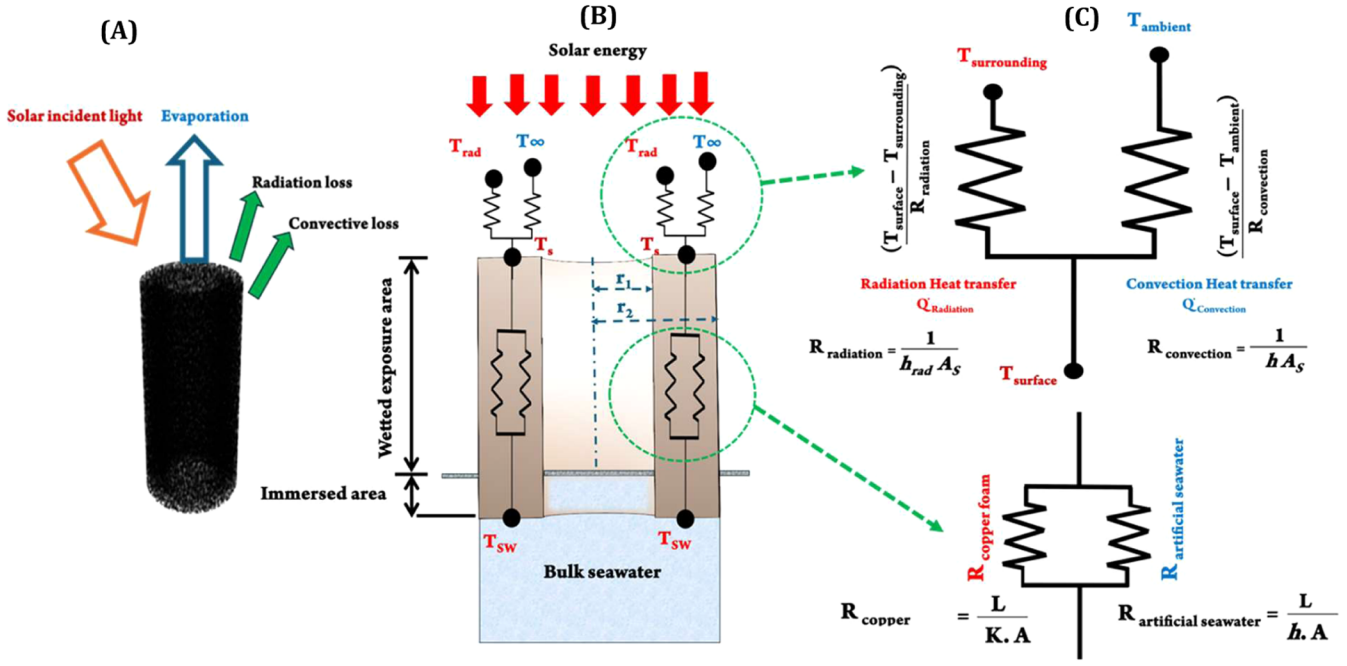

Figure 8. (A) Net energy balance of the evaporator. (B) A model depicting the thermal resistance pathway from solar input to bulk artificial seawater. (C) The upper section illustrates thermal resistances from radiation and convective heat transfer, while the lower section represents thermal resistances within the copper foam skeleton and artificial seawater.

literature[23,34,37,92−94] as well as investigations on the effect of different structure heights in cylindrical shapes.[37,95] Beyond structural optimization, recent developments can also be explored, such as the integration of solar steam evaporation with power generation. For instance, a carbon foam-based bifunctional evaporator—fabricated from waste polyester via a ball-milling-assisted carbonization method—has demonstrated remarkable performance. This innovative design enhances water transport, promotes strong light absorption, and achieves an evaporation rate of 3.03 $kg{\cdot}m^{-2}{\cdot}h^{-1}$ with a high efficiency of 99.4%. Moreover, it enables continuous electricity generation, delivering an output of 0.33 V and 14.4 μA.[96]

Thermal Resistance. Thermal resistance analysis is crucial for understanding the temperature differences through the evaporators and more thermal control. This temperature difference is essential for determining energy losses, particularly due to radiation at the outermost surface. The bulk seawater temperature (T_{SW}) inside the insulated beaker remains at 22 °C, while the temperature at the top surface of the structure (T_S) remains relatively stable, ranging between 29 and 30 °C, and the side wall remains stable at 25 °C, as shown previously in Figure 7 C(a, b), where (a) represent side area and (b) for top area. The temperature near the surrounding surface averages around 40 °C. An ambient temperature of 26 °C is used to estimate convective heat loss. The net energy in Figure 8A and the thermal resistance model shown in Figure 8 aim to demonstrate controllable heat distribution within the internal structure and the potential utilization of circumferential heat around the evaporation process. For the calculations, the following equations were used to determine the net energy and heat loss.

$$Q_{incident} = Q_{evaporation} + Q_{conduction} + Q_{convective} + Q_{radiation} \quad (2)$$

$$Q_{evaporation} = \dot{m}h_{LV} \quad (3)$$

$$Q_{conduction} = K\left(\frac{T_S - T_W}{L}\right) \quad (4)$$

$$Q_{convection} = hA(T_{surface} - T_\infty) \quad (5)$$

$$Q_{radiation} = A\sigma\varepsilon(T^4_{surface} - T^4_{surrounding}) \quad (6)$$

where, $\dot{m}$ is the mass flow rate ($kg{\cdot}s^{-1}$); h_{LV} is the latent heat of vaporization ($J{\cdot}kg^{1-}$); K is the thermal conductivity of the material ($W{\cdot}m^{-1}{\cdot}k^{-1}$); T_S and T_{SW} are the surface and bulk water temperature (K) respectively; L is the characteristic length; h is the convective heat transfer coefficient ($W{\cdot}m^{-2}{\cdot}k^{-1}$); A is the surface area; T_∞ is the ambient temperature; ε is the emissivity of a surface; σ is Stefan−Boltzmann constant (5.67×10^{-8} $W{\cdot}m^{-2}{\cdot}K^{-4}$). It is important to note that in the case of the double layer, we must consider the thermal conductivity of both layers, $K1$ and $K2$, as well as the convective heat transfer coefficients, $h1$ and $h2$ ($K1 = K2$, $h1 = h2$). These factors are crucial for determining the overall heat loss. Further validation of heat resistance, as shown in Figure 8, is supported by calculations of heat losses due to convection, radiation, and conduction, based on all measured temperatures on the top and side of the samples. These details are provided in Table S3 of the Supporting Information and discussed in the Supporting Note section.

CONCLUSIONS

In conclusion, this study demonstrates the potential of vertically etched porous copper foam as an efficient photothermal material for solar interfacial evaporators. We began by comparing single-layer tubes of etched copper foam to double-layer configurations, leveraging light reflection properties to enhance performance. The unique light-trapping design, combined with the hierarchical nano/microscale structure of the foam skeleton, significantly enhances solar absorption and ensures effective salt management.

https://doi.org/10.1021/acs.langmuir.5c01314
Langmuir 2025, 41, 11794−11805

The design incorporates a small ICPC at the center of a copper foam tube with a nanoscale hierarchical surface structure. This configuration facilitates multiple reflections, significantly boosting solar absorption at various angles of incidence, leading to an evaporation rate of 17.15 $kg{\cdot}m^{-2}{\cdot}h^{-1}$. We investigated and applied 3D vertically etched porous copper foam with various designs as interfacial evaporators, aimed at efficiently capturing solar energy and utilizing environmental heat. This heat transfer extends through the foam skeleton and around its circumference, as heat flux from the surroundings also impacts the perimeter of the cylinder. Overall, our tube design effectively overcomes existing challenges, ensuring optimal thermal performance throughout the entire structure.

The incorporation of a small amount of metal provides a cost-effective approach to managing heat distribution by utilizing environmental heat and controlling heat transfer, rather than constructing the entire structure from cone-shaped materials. Heat is sourced from both the top (solar radiation) and inside the tube (reflected light and stored heat). This combination, along with ambient heat, optimizes evaporation efficiency across the evaporator's foam structure, allowing solar radiation to penetrate the copper foam for volumetric absorption. While laboratory results are promising, further research is essential to address practical challenges such as material degradation, salt resistance, and vapor condensation in real-world conditions. By tackling these issues, more efficient, durable, and economical solar desalination and vapor generation systems can be developed, contributing to sustainable water management solutions. Importantly, this work represents a reproducible research approach that can be further refined for large-scale applications and adapted by replacing materials with more cost-effective alternatives. Therefore, further development is needed to fully realize its potential in practical applications. Additional work is required to conduct mechanical testing (e.g., compressive strength, fatigue resistance) and to enhance the system by integrating a condensation mechanism, as well as extending the study to 50 or more cycles under varying salinity levels in future investigations.

■ ASSOCIATED CONTENT

Supporting Information

The Supporting Information is available free of charge at https://pubs.acs.org/doi/10.1021/acs.langmuir.5c01314.

Laboratory etching process of copper foam and copper foil; optimization steps of the final structure; self-cleaning of salt outside the evaporator; tables of heat loss calculations, including the estimated cost analysis of materials and chemicals used; mass loss (evaporation) rate calculations of the samples; and heat loss calculations (PDF)

■ AUTHOR INFORMATION

Corresponding Authors

Husam Eltigani − *Metallurgy and Materials Science Research Institute (MMRI), Chulalongkorn University, Bangkok 10330, Thailand;* orcid.org/0000-0003-0477-0259; Email: husamhussein.i@chula.ac.th

Yuttanant Boonyongmaneerat − *Metallurgy and Materials Science Research Institute (MMRI), Chulalongkorn University, Bangkok 10330, Thailand*; Email: Yuttanant.B@chula.ac.th

Complete contact information is available at: https://pubs.acs.org/10.1021/acs.langmuir.5c01314

Notes

The authors declare no competing financial interest.

■ ACKNOWLEDGMENTS

This work is financially supported by Rachadapisek Sompote Fund, Graduate School, Chulalongkorn University, Metallurgy and Materials Science Research Institute (MMRI), Chulalongkorn University and Ministry of Higher Education, Science, Research and Innovation (MHESI).

■ REFERENCES

(1) Chang, C.; Liu, M.; Li, L.; et al. Salt-rejecting rGO-coated melamine foams for high-efficiency solar desalination. *J. Mater. Res.* **2022**, *37* (1), 294−303.

(2) Singh, S. C.; ElKabbash, M.; Li, Z.; et al. Solar-trackable superwicking black metal panel for photothermal water sanitation. *Nat. Sustainability* **2020**, *3* (11), 938−946.

(3) Bonaccorsi, L.; Freni, A.; Proverbio, E.; et al. Zeolite coated copper foams for heat pumping applications. *Microporous Mesoporous Mater.* **2006**, *91* (1−3), 7−14.

(4) Subhadarshini, S.; Singh, R.; Mandal, A.; et al. Silver nanodot decorated dendritic copper foam as a hydrophobic and mechano-chemo bactericidal surface. *Langmuir* **2021**, *37* (31), 9356−9370.

(5) Wang, S.; Wang, W.; Yue, L.; et al. Hierarchical Cu2O nanowires covered by silver nanoparticles-doped carbon layer supported on Cu foam for rapid and efficient water disinfection with lower voltage. *Chem. Eng. J.* **2020**, *382*, No. 122855.

(6) Zhao, S.; Xia, M.; Zhang, Y.; et al. Novel oil-repellent photothermal materials based on copper foam for efficient solar steam generation. *Sol. Energy Mater. Sol. Cells* **2021**, *225*, No. 111058.

(7) Zhao, Z.; Wang, C.; Wei, D.; Wang, F. Condensation device design represents a critical step for solar-driven water evaporation toward practical applications. *Cell Rep. Phys. Sci.* **2024**, *5*, No. 101794, DOI: 10.1016/j.xcrp.2024.101794.

(8) Chen, Z.; Qian, Z.; Wu, Y.; et al. Micro-interface engineering of CuO-coated copper mesh for enhanced solar absorption and localized heating in continuous seawater desalination. *Sol. Energy Mater. Sol. Cells* **2025**, *282*, No. 113373.

(9) Ye, Q.; Tao, P.; Chang, C.; et al. Form-stable solar thermal heat packs prepared by impregnating phase-changing materials within carbon-coated copper foams. *ACS Appl. Mater. Interfaces* **2019**, *11* (3), 3417−3427.

(10) Yang, S.; Liu, J.; Hoque, M. J.; et al. A Critical Perspective on Photothermal De-Icing. *Adv. Mater.* **2025**, *37* (7), No. 2415237.

(11) Wang, H.; Wen, X.; Liu, K.; et al. Interfacial solar-driven steam and electricity co-generation using Hydrangea-like graphene by salt-assisted carbonization of waste polylactic acid. *SusMat* **2024**, *4* (6), No. e242.

(12) Wilson, H. M.; Wani, T. A.; Lee, S. J. All-Day, All-Weather Desalination Using a Contactless Evaporator with Antisalt Fouling Property. *ACS Appl. Mater. Interfaces* **2024**, *16* (50), 69450−69458.

(13) Lv, F.; Miao, J.; Hu, J.; Orejon, D. 3D solar evaporation enhancement by superhydrophilic copper foam inverted cone and graphene oxide functionalization synergistic cooperation. *Small* **2023**, *19* (30), No. 2208137.

(14) Zhang, C.; Liang, H. Q.; Xu, Z. K.; Wang, Z. Harnessing solar-driven photothermal effect toward the water−energy nexus. *Adv. Sci.* **2019**, *6* (18), No. 1900883.

(15) Ganeshan, A.; Jha, N. Solar-driven water purification technologies. *Int. J. Adv. Eng. Sci. Appl. Math.* **2025**, 1−21.

(16) Wang, B.; Wang, C.; Li, Y.; et al. Bionic design: insights from nature for solar interfacial evaporators. *Energy Environ. Sci.* **2025**, *18*, 3432−3461, DOI: 10.1039/D4EE05898D.

(17) Ren, J.; Gu, T.; Ma, S.; et al. Key factor in continuous salt harvesting via solar interfacial evaporation: Water supply to evaporation ratio. *Desalination* **2025**, *607*, No. 118800.

(18) Shi, C.; Zhang, P.; Wang, Y.; et al. Highly Efficient, Salt-Resistant, and Chemically Durable Solar Evaporator for the Purification of Industrial High-Salinity Wastewater. *Adv. Funct. Mater.* **2025**, No. 2501165.
(19) Wu, Z.-W.; Yang, H.-C. Solar energy technologies for desalination and utilization of hypersaline brines. *Sustainable Energy Fuels* **2025**, *9*, 673−692, DOI: 10.1039/D4SE01552E.
(20) Shen, Y.; Zhang, R.; Hou, G.; et al. Sunflower-inspired smart evaporator with omnidirectional solar tracking for highly enhanced energy-capturing and sustainable freshwater harvesting. *Chem. Eng. J.* **2025**, *503*, No. 157917.
(21) Ma, J.; Sun, X.; liu, Y.; et al. Bio-inspired Micro-architecturing of 3D Aerogel Evaporator for Highly Efficient Solar Seawater Desalination. *Nano Energy* **2025**, *137*, No. 110781.
(22) Wu, J.-M.; Zhao, Y. Y.; Chen, H. D.; et al. Pompon dahlia-inspired 3D architecture for omnidirectional light harvest and high-efficiency solar steam generation. *Chem. Eng. J.* **2025**, *506*, No. 160045.
(23) Li, X.; Li, J.; Lu, J.; et al. Enhancement of interfacial solar vapor generation by environmental energy. *Joule* **2018**, *2* (7), 1331−1338.
(24) Wang, Z. Y.; Zhu, Y.; Chen, Y.; et al. Bioinspired Aerogel with Vertically Ordered Channels and Low Water Evaporation Enthalpy for High-Efficiency Salt-Rejecting Solar Seawater Desalination and Wastewater Purification. *Small* **2023**, *19* (19), No. 2206917.
(25) Mao, K.; Zhang, Y.; Tan, S. C. Functionalizing solar-driven steam generation towards water and energy sustainability. *Nat. Water* **2025**, *3*, 144−156.
(26) Zhang, Q.; Ren, L.; Xiao, X.; et al. Vertically aligned Juncus effusus fibril composites for omnidirectional solar evaporation. *Carbon* **2020**, *156*, 225−233.
(27) Chen, Z.; Dong, M.; Wang, C. Passive interfacial photothermal evaporation and sky radiative cooling assisted all-day freshwater harvesting: System design, experiment study, and performance evaluation. *Appl. Energy* **2024**, *355*, No. 122254.
(28) Zhang, X.; Cong, H.; Ma, L.; et al. Jellyfish-inspired sustainable and facile porous zwitterionic hydrogel sponge for efficient solar thermal desalination and water purification. *Chem. Eng. J.* **2024**, *487*, No. 150754.
(29) Li, H.-C.; Li, H. N.; Zou, L. Y.; et al. Vertically π-extended strong acceptor unit boosting near-infrared photothermal conversion of conjugated polymers toward highly efficient solar-driven water evaporation. *J. Mater. Chem. A* **2023**, *11* (6), 2933−2946.
(30) Sun, M.; Xu, L.; Shao, Y.; et al. Efficient Double-Layer Evaporators with Adjustable Pores for Sustainable Solar Evaporation. *Langmuir* **2025**, *41*, 3662−3674, DOI: 10.1021/acs.langmuir.4c04882.
(31) Wang, B.; Cheng, H.; Zhu, H.; Qu, L. Hierarchically Structured Hydrogels for Rapid Solar Vapor Generation With Super Resistance to Salt. *Adv. Funct. Mater.* **2025**, No. 2500459.
(32) Sun, Y.; Zhao, Z.; Zhao, G.; et al. High performance carbonized corncob-based 3D solar vapor steam generator enhanced by environmental energy. *Carbon* **2021**, *179*, 337−347.
(33) Wani, T. A.; Garg, P.; Bera, A. An environmental pollutant to an efficient solar vapor generator: an eco-friendly method for freshwater production. *Mater. Adv.* **2021**, *2* (12), 3856−3861.
(34) Dang, C.; Chen, M.; Huang, L.; et al. A multichannel photothermal rod for antigravity water transportation and high-flux solar steam generation. *J. Mater. Chem. A* **2022**, *10* (35), 18116−18125.
(35) Liu, H.; Zhai, W. Rattan-Inspired Salt-Resistant Elevated 3D Solar Evaporators with Multi-Scale Aligned Fluid Channels for Efficient and Continuous Seawater Desalination. *Adv. Funct. Mater.* **2025**, No. 2417169.
(36) Hou, L.; Li, S.; Qi, Y.; et al. Advancing Efficiency in Solar-Driven Interfacial Evaporation: Strategies and Applications. *ACS Nano* **2025**, *19*, 9636−9683, DOI: 10.1021/acsnano.4c16998.
(37) Finnerty, C. T. K.; Menon, A. K.; Conway, K. M.; et al. Interfacial solar evaporation by a 3D graphene oxide stalk for highly concentrated brine treatment. *Environ. Sci. Technol.* **2021**, *55* (22), 15435−15445.
(38) Song, Y.; Fang, S.; Xu, N.; Zhu, J. Solar-driven interfacial evaporation technologies for food, energy and water. *Nat. Rev. Clean Technol.* **2025**, *1* (1), 55−74.
(39) Girichandran, N.; Saedy, S.; Kortlever, R. Electrochemical CO2 reduction on a copper foam electrode at elevated pressures. *Chem. Eng. J.* **2024**, *487*, No. 150478.
(40) Elshaer, A. M.; Soliman, A.; Kassab, M.; et al. Experimental investigations on copper foam/PCM composite-based thermal control hardware (TCH) using foam samples with different pore sizes under intermittent thermal conditions. *J. Energy Storage* **2023**, *72*, No. 108320.
(41) Lee, S.; Lee, H.; Jun, Y. J.; Lee, H. Hybrid battery thermal management system coupled with paraffin/copper foam composite phase change material. *Appl. Energy* **2024**, *353*, No. 122043.
(42) Peng, S.; Xu, L.; Deng, S.et al. Integrated Microcavity Network Enhances Fluid-Thermal Transport for Efficient Multi-Heat Source Evaporation Management *ACS ES&T Eng.* 2025 DOI: 10.1021/acsestengg.5c00012.
(43) Jia, D.; Wang, K.; Wang, X.; et al. Surface Engineering of Copper Foam to Construct a Hierarchical Heterostructure for High Energy Efficient Supercapacitors. *Small* **2025**, *21* (3), No. 2408572.
(44) Xu, N.; Li, J.; Wang, Y.; et al. A water lily−inspired hierarchical design for stable and efficient solar evaporation of high-salinity brine. *Sci. Adv.* **2019**, *5* (7), No. eaaw7013.
(45) Yu, B.; Wang, Y.; Zhang, Y.; Zhang, Z. Self-Supporting Nanoporous Copper Film with High Porosity and Broadband Light Absorption for Efficient Solar Steam Generation. *Nano-Micro Lett.* **2023**, *15* (1), No. 94.
(46) Eltigani, H.; Boonyongmaneerat, Y. Modifications of the wetting characteristics of electrodeposited porous copper by controlling the plating parameters and storage conditions. *Micron* **2021**, *150*, No. 103140.
(47) Zhang, C.; Chen, G.; Xie, S.; et al. Integrated copper-based Janus thermal system for efficient water harvesting around the clock. *Droplet* **2025**, *4*, No. e152.
(48) Yin, K.; Wu, Z.; Wu, J.; et al. Solar-driven thermal-wind synergistic effect on laser-textured superhydrophilic copper foam architectures for ultrahigh efficient vapor generation. *Appl. Phys. Lett.* **2021**, *118* (21), No. 211905, DOI: 10.1063/5.0050623.
(49) Yao, H.; Zhang, P.; Yang, C.; et al. Janus-interface engineering boosting solar steam towards high-efficiency water collection. *Energy Environ. Sci.* **2021**, *14* (10), 5330−5338.
(50) Cai, W.; Luo, X.; Lian, Z.; et al. Optical-Concentrating Solar Distillation Based on Three-Dimensional Copper Foam Cubes Coated with CuS Nanoparticles and Agarose Gel. *ACS Appl. Mater. Interfaces* **2023**, *15* (16), 20120−20129.
(51) Shi, W.; Dalrymple, R. M.; McKenny, C. J.; et al. Passive water ascent in a tall, scalable synthetic tree. *Sci. Rep.* **2020**, *10* (1), No. 230.
(52) Kaviany, M. *Principles of Heat Transfer in Porous Media*; Springer Science & Business Media, 2012.
(53) Cao, N.; Lu, S.; Yao, R.; et al. A self-regenerating air-laid paper wrapped ASA 3D cone-shaped Janus evaporator for efficient and stable solar desalination. *Chem. Eng. J.* **2020**, *397*, No. 125522.
(54) Bai, B.; Yang, X.; Tian, R.; et al. High-efficiency solar steam generation based on blue brick-graphene inverted cone evaporator. *Appl. Therm. Eng.* **2019**, *163*, No. 114379.
(55) Li, H.; Jia, D.; Ding, M.; et al. Robust 3D graphene/cellulose nanocrystals hybrid lamella network for stable and highly efficient solar desalination. *Sol. RRL* **2021**, *5* (8), No. 2100317.
(56) Wang, Y.; Wu, X.; Gao, T.; et al. Same materials, bigger output: A reversibly transformable 2D−3D photothermal evaporator for highly efficient solar steam generation. *Nano Energy* **2021**, *79*, No. 105477.
(57) Liu, C.; Peng, Y.; Huang, C.; et al. Bioinspired superhydrophobic/superhydrophilic janus copper foam for on-demand oil/water separation. *ACS Appl. Mater. Interfaces* **2022**, *14* (9), 11981−11988.
(58) Ma, C.; Zhu, L.; Qiao, X.; et al. Ni-doped brochantite@ copper hydroxide hierarchical structures on copper mesh with ultrahigh oil-resistance for high-efficiency oil/water separation. *Surf. Coat. Technol.* **2021**, *406*, No. 126642.
(59) Li, H.; Zhang, Z.; Ren, Z.; et al. A quadruple biomimetic hydrophilic/hydrophobic Janus composite material integrating Cu

(OH) 2 micro-needles and embedded bead-on-string nanofiber membrane for efficient fog harvesting. *Chem. Eng. J.* **2023**, *455*, No. 140863.
(60) Thomsen, L.; Johra, H.; Yue, Y.; Østergaard, M. B. Anomaly in the relation between thermal conductivity and crystallinity of silicate glass-ceramics. *Ceram. Int.* **2024**, *50* (6), 9908−9912.
(61) Park, K.; Noh, K.-J.; Lee, K.-S. Transport phenomena in the thin-film region of a micro-channel. *Int. J. Heat Mass Transfer* **2003**, *46* (13), 2381−2388.
(62) Xuemin, G.; Peng, Y.; Yanfen, W. How to reduce enthalpy in the interfacial solar water generation system for enhancing efficiency? *Nano Energy* **2024**, *123*, No. 109434.
(63) Wei, D.; Wang, C.; Zhang, J.; et al. Water Activation in Solar-Powered Vapor Generation. *Adv. Mater.* **2023**, *35* (47), No. 2212100.
(64) Wang, G.; Ma, F.; Zhu, L.; et al. Bioinspired slippery surfaces for liquid manipulation from tiny droplet to bulk fluid. *Adv. Mater.* **2024**, *36* (37), No. 2311489.
(65) Singh, S. C.; Vorobyev, A.; ElKabbash, M.; et al. Maintenance-free ultrahigh energy-and water-efficient evaporative cooling with superwicking, anti-scaling, and antifouling surface. *Cell Rep. Phys. Sci.* **2025**, *6*, No. 102518, DOI: 10.1016/j.xcrp.2025.102518.
(66) Sun, X.; Miao, J.; Wang, H.; et al. Multiscale Heat and Mass Transport Optimization for Solar-Driven Interfacial Evaporation: Opportunities and Challenges for Industrial Applications. *Small* **2025**, No. 2502639.
(67) Wen, Y.; Deng, S.; Xie, Q.; et al. Nanofibrous Hydrogel with Highly Salt-Resistant Radial/Vertical-Combined Structure for Efficient Solar Interfacial Evaporation. *Small* **2025**, No. 2411780.
(68) Park, J.; Tsogbayar, D.; Lim, M.; et al. High-Efficiency Heat Dissipation Coating Implemented with a Stepwise Thermally Conductive Pathway Using a Parylene-Nanocoated Thermal Filler. *ACS Appl. Polym. Mater.* **2025**, *7*, 1421−1430, DOI: 10.1021/acsapm.4c03163.
(69) Al-Sharafi, A.; Yilbas, B. S.; Ali, H.; AlAqeeli, N. A water droplet pinning and heat transfer characteristics on an inclined hydrophobic surface. *Sci. Rep.* **2018**, *8* (1), No. 3061.
(70) Daniel, D.; Vuckovac, M.; Backholm, M.; et al. Probing surface wetting across multiple force, length and time scales. *Commun. Phys.* **2023**, *6* (1), No. 152.
(71) Bai, H.; Zhao, T.; Cao, M. Interfacial fluid manipulation with bioinspired strategies: special wettability and asymmetric structures. *Chem. Soc. Rev.* **2025**, *54*, 1733−1784, DOI: 10.1039/D4CS01073F.
(72) Liu, C.-H.; Xu, L.; Wang, Z. Y.; et al. Photothermal evaporator with low enthalpy of evaporation and hierarchical porous structure for efficient photothermal evaporation. *Chem. Eng. J.* **2025**, *512*, No. 162282.
(73) Ho, G. W.; Yamauchi, Y.; Hu, L.; et al. Solar evaporation and clean water. *Nat. Water* **2025**, *3*, 131−134.
(74) Xu, H.; Zhu, Y.; Xu, Z.; et al. Developing solar evaporation technologies of the future. *Cell Rep. Phys. Sci.* **2025**, *6* (1), No. 102313, DOI: 10.1016/j.xcrp.2024.102313.
(75) Cha, H.; Kim, M. K.; Chang, H. C.; et al. Pinning-Induced Microdroplet Self-Transport. *ACS Nano* **2025**, *19*, 11049−11057, DOI: 10.1021/acsnano.4c16960.
(76) Liu, J.; Shen, Y.; Ma, Q.; et al. Friction characteristics of rapid spreading surface with annular microtexture at reciprocating contact interface. *Appl. Surf. Sci.* **2025**, *690*, No. 162649.
(77) Wang, T.; Hou, J.; Wang, M.; et al. Fluid Control on Bionics-Energized Surfaces. *ACS Nano* **2025**, *19* (8), 7601−7616.
(78) Wang, Z.; Jiang, L.; Heng, L. Liquid Adhesion Regulation on Bioinspired Slippery Surfaces: From Theory to Application. *ACS Nano* **2025**, *19*, 13549−13566, DOI: 10.1021/acsnano.5c00222.
(79) Liu, X.; Yang, J.; Zou, Q.; et al. Enhancing Liquid−Vapor Phase-Change Heat Transfer with Micro/Nano-Structured Surfaces. *ACS Nano* **2025**, *19*, 9513−9589, DOI: 10.1021/acsnano.4c15277.
(80) Wang, X.; Xia, N.; Pan, C.; et al. Beyond surface tension-dominated water surface jumping. *Nat. Commun.* **2025**, *16* (1), No. 3034.
(81) Fauconnier, M.; Karunakaran, B.; Drago-González, A.; et al. Fast capillary waves on an underwater superhydrophobic surface. *Nat. Commun.* **2025**, *16* (1), No. 1568.
(82) Chen, C.; Duru, P.; Joseph, P.; et al. Control of evaporation by geometry in capillary structures. From confined pillar arrays in a gap radial gradient to phyllotaxy-inspired geometry. *Sci. Rep.* **2017**, *7* (1), No. 15110.
(83) Holtzman, R. Effects of pore-scale disorder on fluid displacement in partially-wettable porous media. *Sci. Rep.* **2016**, *6* (1), No. 36221.
(84) Liu, L.; Fu, C.; Li, S.; et al. Superspreading Surface with Hierarchical Porous Structure for Highly Efficient Vapor−Liquid Phase Change Heat Dissipation. *Small* **2024**, No. 2403040.
(85) Manetti, L. L.; Moita, A. S. O. H.; de Souza, R. R.; Cardoso, E. M. Effect of copper foam thickness on pool boiling heat transfer of HFE-7100. *Int. J. Heat Mass Transfer* **2020**, *152*, No. 119547.
(86) Tian, Y.; Chen, S.; Wang, R.; et al. Immersion Phase-Change Liquid Cooling Devices Based on Copper Microgroove/Nanocone Composite Structure. *Nano Lett.* **2025**, *25*, 1932−1938, DOI: 10.1021/acs.nanolett.4c05588.
(87) Zhang, C.; Wang, H.; Huang, Y.; et al. Immersion liquid cooling for electronics: Materials, systems, applications and prospects. *Renewable Sustainable Energy Rev.* **2025**, *208*, No. 114989.
(88) Sun, Y.; Tan, X.; Xiang, B.; et al. Solar-driven interfacial evaporation for sustainable desalination: Evaluation of current salt-resistant strategies. *Chem. Eng. J.* **2023**, *474*, No. 145945.
(89) Wang, Y.; Wei, T.; Wang, Y.; et al. Quasi-waffle solar distiller for durable desalination of seawater. *Sci. Adv.* **2024**, *10* (22), No. eadk1113.
(90) Liu, J.; Ruan, W.; Zhang, H.; et al. Highly Efficient Porous Glass Solar Water Evaporator. *Adv. Funct. Mater.* **2025**, *35* (7), No. 2415394.
(91) Lu, T.; Li, X.; Lv, W.et al. Durable and highly absorptive ant-nest structured superhydrophobic sponge for efficient de-icing and interfacial evaporation in polar environments *Mater. Horiz.* 2025 DOI: 10.1039/D4MH01887G.
(92) Anukunwithaya, P.; Koh, J. J.; Chuan Yeo, J. C.; et al. A self-regenerating 3D sponge evaporator with a tunable porous structure for efficient solar desalination. *J. Mater. Chem. A* **2022**, *10* (29), 15743−15751.
(93) Kim, D. K.; Philip, L.; McDonagh, A.; et al. Recent Advances in High-Rate Solar-Driven Interfacial Evaporation. *Adv. Sci.* **2024**, No. 2401322.
(94) Wu, X.; Gao, T.; Han, C.; et al. A photothermal reservoir for highly efficient solar steam generation without bulk water. *Sci. Bull.* **2019**, *64* (21), 1625−1633.
(95) Li, H.; Liu, X.; Niu, X.; et al. Mixed temperature gradient evaporator for solar steam generation. *Cell Rep. Phys. Sci.* **2022**, *3* (9), No. 101014, DOI: 10.1016/j.xcrp.2022.101014.
(96) Hu, G.; Liu, H.; Liu, K.; et al. All-In-One Carbon Foam Evaporators for Efficient Co-Generation of Freshwater and Electricity. *Adv. Funct. Mater.* **2025**, No. 2423781.

https://doi.org/10.1021/acs.langmuir.5c01314
Langmuir 2025, 41, 11794−11805